# Macrophage migration inhibitory factor is a valid drug target at the intersection of herpes simplex virus 1 replication and Alzheimer´s disease-relevant cellular pathology

Andreas Müller-Schiffmann[1], Felix Torres[2], Anatolly Kitaygorodskyy[3], Anand Ramani[4], Argyro Alatza[5], Sarah Tschirner[1], Ingrid Prikulis[1], Shaofeng Yu[3], Debendranath Dey[3], Verian Bader[1], Annemieke Rozemuller[6], Selina Wray[5], Jay Gopalakrishnan[4], Roland Riek[2], Vishwanath R. Lingappa[3], Carsten Korth[1]*

[1]Department Neuropathology, Heinrich Heine University Düsseldorf, 40225 Düsseldorf, Germany
[2]Department Physical Chemistry, Federal Research Institute, Zurich, Switzerland
[3]Prosetta Biosciences, San Francisco, USA
[4]Department Human Genetics, Heinrich Heine University, 40225 Düsseldorf, Germany
[5]Department of Neurodegenerative Disease, UCL Queen Square Institute of Neurology, London WC1N 1PJ, United Kingdom
[6]Department Pathology, VUMC Amsterdam, 1081HV Amsterdam, The Netherlands

*corresponding author
Carsten Korth, MD PhD
Department Neuropathology
Heinrich Heine University Düsseldorf
Moorenstrasse 5
40225 Düsseldorf
Tel +49 211 8116153
Email: ckorth@hhu.de

**Abstract**

Herpes virus infections are endemic and ubiquitous. While only rarely leading to overt encephalitis, subchronic or latent infections have been associated to a variety of conditions, including Alzheimer's disease (AD). The cellular consequences of herpes virus infection are determined by the host proteins recruited during virus replication and assembly. Identifying such virus-recruited host proteins therefore allows the interrogation fundamental cellular events leading to associated "sporadic" diseases.

A host protein-targeted small molecule drug highly active against herpes simplex virus 1 (HSV-1) infection in human brain organoids and cell lines was identified to interact with macrophage migration inhibitory factor (MIF) where it acted by intercalating between MIF units within a trimer, as determined by nuclear magnetic resonance (NMR). MIF knockout cells showed a decreased viral antigen/titer ratio corroborating its role in virus assembly.

From post-mortem brain homogenates of patients with Braak 6-staged AD the small molecule lead compound specifically eluted a MIF subpopulation that correlated with the oxidized conformer of MIF (oxMIF). HSV-1 led to an increase in tau phosphorylation at distinct residues, and the lead compound decreased tau phosphorylation in recombinant cell lines expressing mutant tau and in neuron-differentiated iPSCs also in the absence of HSV-1 infection.

We conclude that MIF is a cellular host factor involved in HSV-1 replication and a drug target with antiviral efficacy. At the same time, MIF also plays a role in tau phosphorylation and is enriched in an oxidized conformation in brains of AD patients. MIF thus presents as a molecular link connecting HSV-1 infection and cellular pathology characteristic of neurodegenerative diseases involving aberrant tau phosphorylation.

## Introduction

The discovery of novel antiviral drugs has so far primarily focused on virus-encoded proteins, which is intuitive since the virus is the causative agent for virus-induced diseases. Viral replication *in vivo*, however, is dependent on cellular host factors, which therefore provide an alternative target, albeit an elusive one. Virus dependence on host factors is not limited to nucleic acid replication but includes capsid assembly, which is catalyzed in cells by virus-recruited proteins exploiting their moonlighting functions, and can be reconstituted in cell free systems (Lingappa et al., 2013a; Lingappa et al., 2013b; Reed et al., 2021; Selvarajah et al., 2021). The establishment of cell-free systems catalyzing capsid formation enabled novel drug screens (Lingappa et al 2013b). Drugs targeting these cellular host factors have several advantages: First, resistance development is greatly diminished since the selection of host factors is on a much longer time scale than viral replication cycles. Second, the host protein targets of these drugs can give clues as to host proteins essential for virus-induced cellular pathology, which ultimately causes clinical disease (Müller-Schiffmann et al., 2020). Third, the ability to target a small subpopulation of specific host proteins recruited for their moonlighting functions (Jeffery, 2020) is unlikely to affect their canonical functions in cellular homeostasis. Solutions combining these advantages cannot reasonably be obtained by rational design but can be gleaned from viruses that achieved those innovations by natural selection over deep evolutionary time (Muller-Schiffmann et al., 2020).

Herpes simplex virus (HSV-1) is a human pathogenic virus, which in rare cases causes overt encephalitis but endemically stays latent in sensory neurons causing reactivation upon a variety of conditions. Reactivation of latent herpes virus infection has been associated with AD even though the molecular mechanisms responsible for this connection remain unknown (Eimer et al., 2018; Itzhaki et al., 1997; Lovheim et al., 2015; Wozniak et al., 2009).

We here present the discovery of a drug highly active against HSV-1 in human brain organoids and human cell lines displaying a robust structure-activity relationship (SAR). We demonstrate that the lead compound targets a multiprotein complex comprising macrophage migration inhibitory factor (MIF). We validate MIF as a host factor by CRISPR/Cas9 knockout experiments and demonstrate its role in AD-like cellular pathology.

## Results

### *Anti-HSV1 activity of a novel compound directed to host factors assisting in HSV1 assembly*

From a cell-free capsid assembly assay screen of a chemical library (Lingappa et al., 2010; Lingappa et al., 2013b) similar to what we have successfully described for rabies virus (Lingappa et al., 2013a), human immunodeficiency virus (HIV) (Reed et al., 2021), and respiratory viruses (Selvarajah et al., 2021), an early lead compound (1.32) was identified with activity in inhibiting herpes virus capsid assembly. This compound was subsequently optimized for activity over seven generations to lead to an improved compound 7.25 that inhibited HSV-1 replication in a dose-dependent manner in HSV-1-infected Vero cells both in a standard plaque assay (**Figure 1A**) and in an in-cell ELISA (**Figure 1B**) with an $EC_{50}$ of 32 nM or 25 nM, respectively, and an $LD_{50}$ of 1.12 µM (**Supplementary Figure 1**). The compound was also active in differentiated primary neuron-like human dopaminergic LUnd Human MESencephalic (LUHMES) cells (**Figure 1C,D**), as well as in differentiated 60d human brain organoids (**Figure 1E, F**) where it also lowered HSV-1-induced neurotoxicity (**Figure 1G**). This indicated solid antiherpetic activity in several independent systems, including human primary-like cells. The compound also displayed a solid structure-activity-relationship (SAR) as measured by an in-cell ELISA in Vero cells (**Table 1, Supplementary Figure 2**).

### *Identification of cellular host proteins targeted by active compound*

In order to determine the cellular target of 7.25, we performed drug resin-affinity chromatography (DRAC) with immobilized original compound 1.32 (**Supplementary Figure 3A**). We used pig brain lysates (by availability) as material and, after washing, the final binding proteins were eluted with an excess of free 1.32 (200 µM). The eluate was analyzed by mass spectrometry followed by peptide fingerprinting. Several proteins were identified, some of them having been mentioned in the context of HSV1 or AD-related research (**Table 2**): macrophage migration inhibitory factor (MIF; (Petralia et al., 2020)), copper binding protein (cutA; (Hou P et al., 2015)), glutathione-S-transferase Pi1 (GSTP1; (Wang, 2015)), peroxiredoxin 2 (PRDX2; (Szeliga, 2020)) and calmodulin-like 3 (CALML3; (Chen et al., 2019)). Even though these results suggested that multiple proteins, or a multiprotein complex, could be ligands of active compound, we focused on MIF because of its known role in infection and neurodegenerative disorders (Petralia et al., 2020). We validated the precipitation of MIF in SH-SY5Y neuroblastomacells (**Supplementary Figure 3B**) as well as in human brains (see below). In order to analyze effects of 7.25 in a cellular model for

neurodegenerative diseases (see below) we generated a neuroblastoma-derived cell line stably overexpressing human tau (2N4R) including the familial mutation P301S. These cells could efficiently be infected with HSV-1 **(Supplementary Figure 4A)**. When we generated MIF knockout cells by using the CRISPR/Cas9 technique, infectivity as measured in the plaque assay was not changed (**Figure 2A**), whereas HSV-1 antigens accumulated faster in the MIF knockout cell line with increasing moi (most pronounced at a moi of 0.2), thereby increasing the HSV1 antigen/titer ratio and corroborating our hypothesis that HSV1 assembly inhibition leads to an accumulation of non-assembled viral proteins (**Figure 2B).**

Full activity of lead compound 7.25 was also dependent on the presence of MIF. In MIF knockout SH-SY5Y cells (Figure 2A; **Supplementary Figure 4B**) lead compound 7.25 did not exert additional titer-lowering effects indicating that MIF mediates antiherpetic effects of 7.25.

***The NMR structure of MIF with 7.25 reveals its binding site to be at the multimerization interface***

In order to confirm binding of 7.25 to MIF we measured Heteronuclear Single Quantum Coherence (HSQC) spectra of 7.25 with both wildtype MIF and a mutant favoring the oxidized MIF conformation (MIF C81W; (Schinagl et al., 2018; Thiele et al., 2015)) recombinantly expressed and purified from *E. coli* (**Supplementary Figure 5A**). Spectra revealed discrete binding sites (**Supplementary Figure 5B**) suggesting specific binding. An NMR structure of recombinant MIF together with compound 7.25 demonstrated a binding site at the interface of MIF monomers forming a trimer (**Figure 3A, B**).

The $^{15}$N-HSQC spectra of wildtype MIF and MIF C81W, in the presence or absense of 7.25, revealed that 7.25 bound to both MIF species. However, the low alignment between the chemical shifts of the MIF C81W and wildtype MIF did not allow identifying the binding site. It is worth noticing that the resonance and shifts corresponding to the W108 side chain are easily aligned between the MIF species suggesting that the 7.25 binds at the same site or in close proximity.

The structure of wt-MIF-7.25 was calculated using the *N*MR$^2$ protocol as previously described. Hence, two $F_1$-[$^{13}$C,$^{15}$N]-filtered-[$^1$H,$^1$H]-NOESY experiments were measured with 60 and 100 ms mixing times and the cross-peaks corresponding to ligand-proteins were used to derive ligand-protein distant restraints using the initial rates of the normalized NOE

intensity build-up curves. The intermolecular distance restraints involved four different protein aromatic signals and only one protein methyl, consistently with the binding site suggested by the HSQC spectra which is highly populated with aromatic residues. The intermolecular distance restraints were kept semiambiguous, i.e. only the ligand signals were assigned, and the MIF-7.25 complex was calculated with the *N*MR$^2$ software. Finally, the MIF-7.25 complex structure revealed a ligand pose in the aromatic hinge formed at the interface between the different monomers of MIF.

To investigate a potential effect of 7.25 on differential multimerization of wildtype MIF and MIF C81W we performed high-pressure liquid chromatography - multi-angle laser light scattering (HPLC-MALS), where as HPLC column a size exclusion column was used. The HPLC runs were performed for both mutants in the presence or absence of 7.25 (**Supplementary Figure 5C**). The addition of 7.25 did not lead to different retention times in both MIF species. Furthermore, the molecular weight of the observed species was calculated for each sample: wt-MIF: 34140 kDa +/- 2%, wt-MIF + 7.25: 35270 kDa +/- 2%, MIF-C81W: 37890 kDa +/- 7%, and MIF-C81W + 7.25: 37180 kDa +/- 5%, using the Astra software, correcting the Rayleigh ratio by the UV absorbance at 280 nm. These results indicated that MIF is present as a trimer regardless of the interaction with 7.25 and that 7.25 does not perturb the monomer-trimer equilibrium or the oligomerization of both wt-MIF and MIF-C81W (**Supplementary Figure 5C**). The different retention times of wildtype MIF and MIF C81W are likely due to different conformations of both MIF species that have been described (Schinagl et al., 2018). It cannot be excluded that the binding of 7.25 further alters the conformations of MIF species not detectable with the used method.

### *A specific oxidized conformer of MIF is elevated in post mortem brains of patients with Alzheimer's disease*

Since MIF has repeatedly been described to be dysregulated in AD, we pursued the hypothesis that MIF might be one overlapping factor in linking HSV-1-induced cellular changes to AD-like cellular pathology. When we performed DRAC of original compound 1.32 and eluted with more efficient compound 7.25, we observed a stronger pulldown of MIF in post-mortem brain homogenates from patients with AD (**Figure 4A**). Since MIF has been described in two conformers, an oxidized and a reduced form with the oxidized form being the conformer associated to disease (Kassaar et al., 2017; Thiele et al., 2015), we used a monoclonal antibody specific for the oxidized MIF to investigate whether the quantitative difference in the amount of eluted MIF on the background of similar MIF levels in the

homogenate could be due to an increase in the oxidized conformer using a sandwich ELISA. Indeed, oxidized MIF was more abundant in post-mortem brains from AD patients (**Figure 4B**) and the levels of oxMIF positively correlated with the MIF species eluted by DRAC (**Figure 4C**). Braak staging of post-mortem brains has been carefully conducted and was significantly higher in the AD group (**Supplementary Figure 6A, B**). This prompted us to further investigate tau cellular pathology in cell models of tau hyperphosphorylation.

***MIF-dependent changes in tau phosphorylation are prevented by 7.25 in the absence of HSV-1***

HSV-1 infection increased tau phosphorylation at residues Ser202, Thr205 in SH-SY5Y cells overexpressing human tau P301S (**Figure 5A**). Compound 7.25 reduced tau phosphorylation at these sites in a dose-dependent manner in the presence (**Figure 5A**) or absence of virus (**Figure 5B, Supplementary Figure 7A**), and also at other specific phosphorylation sites (**Supplementary Figure 7B**) indicating a specific effect. The well-studied MIF inhibitor ISO-1 (Bacher et al., 2010; Li et al., 2015) did not modulate tau phosphorylation (**Supplementary Figure 7B).** The tau phosphorylation-inhibiting effects displayed a SAR (**Figure 5C**) that correlated with the anti-HSV-1 activity (**Figure 5D**).

The effect of 7.25 on inhibiting tau phosphorylation was MIF dependent since in SH-SY5Y cells overexpressing tau-P301S and that where knocked out for MIF, 7.25 effects on tau phosphorylation were absent (**Figure 5E**).

To corroborate the effects of lead compound 7.25 on tau phosphorylation in primary-like human cells, we treated cortical neurons differentiated from control induced pluripotent stem cells (iPSC) with no known tau mutations with 7.25 for 48h and also did observe reduced phosphorylation at position Ser396 and Ser404 of tau as detected by specific antibody PHF-1 (**Figure 5F**).

## Discussion

Our findings are remarkable in several ways:

1. We here demonstrate that host factors are valid drug targets for efficient HSV-1 antivirals in several *in vitro* assays, including human brain organoids (**Figure 1E**), as we have done previously for other viruses (Lingappa et al., 2013a; Reed et al., 2021; Selvarajah et al., 2021). Unfortunately, the unfavorable pharmacokinetics of lead compound 7.25 with a plasma protein binding of >99% prevented us from conducting *in vivo* studies for its efficiency against HSV-1 infection or tau phosphorylation at this point. Structural analogues with improved bioavailability and similar $EC_{50}$ will have to be carefully developed.

We also showed that the seemingly counterintuitive strategy of first discovering an antiviral compound through a cell-free screen and only afterwards identifying its target by DRAC has the advantage of selecting drugs from a less constrained pharmacological space and, eventually, with more complex mechanisms of action. While lead compound 7.25 clearly bound to MIF (**Figure 3**), MIF knockout cells with no residual MIF immunoreactivity were still able to replicate HSV-1 virus (**Figure 2A**). This could point to MIF being active in HSV-1 replication in conjunction with other factors such as those identified by DRAC (**Table 2**), or that the lead compound has an allosteric binding site in a multiprotein complex only one of them being MIF. The activity of 7.25, however, was dependent on the presence of MIF (**Figure 2A**) thus supporting a role of MIF in the antiherpetic activity. The increased levels of HSV1 glycoprotein in MIF knockout cells (**Figure 2B**) argue that the cell generates more dysfunctional virus likely due to misassembly thus corroborating the suspected mechanism of action of 7.25. This increased HSV-1 antigen/ titer ratio may be a useful parameter when evaluating host-protein targeted compounds by *in vitro* assays.

2. The advantage of identifying host proteins recruited by and involved in virus replication is that the dysfunction of the identified protein allows a more precise delineation the cellular pathology caused by virus infection. We have previously demonstrated that influenza virus infection leads to $\alpha$-synuclein aggregation via the recruitment of host proteins relevant for autophagic flux (Marreiros et al., 2020). In the case of HSV-1 shown here, we demonstrated a link of HSV-1 infection to aberrant tau phosphorylation (**Figure 5**) at residues recognized to play a role in tau-related neurodegenerative diseases such as AD (Augustinack et al., 2002). Supporting our discovery, deficiency of MIF has been previously reported to be associated to attenuated tau phosphorylation *in vivo* (Li et al., 2015). Several links of MIF to neurodegenerative disease and tau phosphorylation-relevant signaling cascades are plausible, such as via its canonical receptor CD74 (Jankauskas et al., 2019), via its

interaction with CXCR4 (Bonham et al., 2018; Martinez-Martin et al., 2015; Rajasekaran et al., 2016), or via MIF-activated microglia (Nasiri et al., 2020).

We have previously outlined how drug discovery in neurodegenerative diseases could take advantage from antivirals targeting host factors provided that both a “sporadic” phenotype and a antiviral-targeted virus share similar cellular pathology (Müller-Schiffmann et al., 2020). The idea is that once the targeted host protein is identified, the binding lead compound can be further developed and improved on its own, that is, irrespective of its original antiviral activity to modulate cellular pathology. Following this line of reasoning, 7.25 may now be the blueprint for another generation of analogues with higher potency to correct aberrant tau phosphorylation. In some cases the specific subset of the protein of interest that may participate in a multiprotein complex could be targeted while leaving those copies of the target protein that are engaged in other functions alone. This ability, developed by the virus through natural selection and signaling pathway manipulation over eons of time, is accessible to humans, given the right tools and assays, as demonstrated by successful use here of a herpes-active drug to provide insight into AD.

3. The long-known epidemiological association between latent herpes virus reactivation and AD (Allnutt et al., 2020; Itzhaki et al., 2020; Lovheim et al., 2015; Readhead et al., 2018; Tzeng et al., 2018) has so far remained unexplained in molecular terms even though several molecular scenarios have been proposed such as a role for Abeta as a cellular defense (Eimer et al., 2018) or an interference of herpes virus with autophagy (Cirone, 2018; Orvedahl et al., 2007). Our results suggest that a small subfraction of MIF, the oxidized MIF conformer, participating in a relevant multi-protein complex, presents a missing molecular link between HSV-1 infection and AD-like cellular pathology, since it has a role both in HSV-1 replication and tau phosphorylation.

4. Our discovery of one particular conformer of MIF, oxidized MIF, that has been described to be proinflammatory and disease-associated in various contexts (Thiele et al., 2015) is upregulated in post-mortem brains from patients with AD (**Figure 4B**) now defines the known role of MIF in AD (Bacher et al., 2010; Petralia et al., 2020) more precisely and corroborates a proinflammatory state in AD.

In conclusion, we have presented a novel, MIF-targeted anti-HSV-1 compound that is also a novel lead compound preventing aberrant tau phosphorylation and hence tau-dependent neurodegenerative disorders like AD independent of HSV-1 infection. MIF, and possibly other proteins in conjunction with MIF in a multiprotein complex, are at the intersection

between HSV-1 replication and AD-like cellular pathology providing a molecular basis for further analyzing the long-known epidemiological connection.

## Materials & Methods

### *1. Chemical synthesis*

Please see Supplementary methods.

### *2. HSV-1 culture and assays*

#### HSV-1 KOS viral stock generation

The HSV-1 KOS strain (ATCC-VR-1493) with $2x10^7$ plaque forming units (pfu)/mL was used to prepare viral stocks after infection of Vero cells (ATCC-CCL-81). A confluent 75-$cm^2$ flask with Vero cells was infected with HSV-1 KOS at a multiplicity of infection (moi) of 0.01 pfu/cell. For this the virus was diluted in 3 mL of 199 medium (Gibco). After incubation for 2 h at 37°C the medium was aspirated and 3 mL of fresh DMEM (Gibco) supplemented with 5% New Born Calf Serum (NBCS; Gibco) was added to the flask. The virus was allowed to replicate for 3 days. Then the virus was released by freeze thawing following 3x sonication for 30 using a Misonix ultrasonic water bath at 100% amplitude. Aliquots of the virus were stored in liquid $N_2$. The virus titer was determined by virus plaque assay.

#### Virus plaque assay

Virus titer determination was carried out in 25-$cm^2$ flasks or 6-well plates with confluent Vero cells. The virus stock was serially diluted in 199 medium. 1 mL of each of the dilutions were added to the Vero cells in duplicates and incubated for 2 h. Then the inoculum was aspirated and DMEM supplemented with 5% NBCS and 7.5 µg/mL human immunoglobulin (Sigma) was added. After two days the cells were washed twice with PBS and fixed with MeOH for 5 min at RT. Then 1:10 diluted KaryoMax Giemsa stain solution (Gibco) was added to the cells and incubated for 20 min at RT. Following washing with water the plaques were counted and the titer calculated.

#### Viral infections

$4x10^5$ Vero cells, $8x10^5$ SH-SY5Y or $2x10^6$ differentiated LUHMES (differentiation day 2) cells were seeded into 12-well plates. After 24h the cells were infected with HSV-1 applying mois as described in the text. After 20h cells were either washed twice with PBS, then lysed in cold PBS/1% NP40 including the cOmplete EDTA-free protease inhibitor cocktail (Roche) or

virus was released by freeze-thawing and ultrasonic treatment for analysis in viral plaque assay (see above).

**In-cell ELISA**

Antiviral activity of the compounds was measured by in-cell ELISA that was adapted from Fabiani et al. (Fabiani et al., 2017). $4x10^4$ Vero cells were seeded in 96-well plates and grown to confluence for 24h. Then, the medium was removed and cells were treated with serially diluted compounds or DMSO added to 50 µL of 199 medium. Thereafter, the cells were infected with 50 µL of HSV-1 (moi of 1) diluted in 199 medium. In parallel cells were infected with serial dilutions of HSV-1 to generate a standard curve. After incubation for 2 h the wells were washed twice with PBS and then 100 µL DMEM plus compound or DMSO were added and the cells were incubated for 24h at 37°C in 5% $CO_2$. At the next day, the cells were washed twice with PBS, fixed with 50 µL of PBS/4% paraformaldehyde (PFA) for 15 min and then permeabilized with 50 µL of PBS/0.1% TX-100 for 5 min at RT. Following blocking with 5% BSA in PBS/0,05% Tween-20 (PBS-T) for 60 min the cells were incubated with 50 µL of anti-HSV-1-gC antibody diluted 1 to 10,000 in PBS-T over night at 4°C. The following day, cells were washed four times with PBS-T and then incubated with Hrp-conjugated goat anti-mouse antibody at a dilution of 1:10,000 in PBS-T for 60 min. Then, cells were washed four times with PBS-T before adding 50 µL of the substrate cocktail (OptEIA). The reaction was stopped after 30 min by adding 50 µL of $H_2SO_4$, and signals were spectrometrically analyzed using a Tecan Safire at 450 nm.

***3. Human organoids and assays***

**Origin and culture**

Organoids were generated from a commercially available hiPSC line (IMR90, Wi Cell). The hiPSCs were maintained on mTeSR medium, under non differentiating conditions for initial expansion. To differentiate into the neural lineage for organoid generation, the hiPSCs were allowed to self-aggregate in 96-well plates for five days using Neural induction medium (Stem cell technologies) as described earlier (Gabriel et al., 2017). The aggregated neurospheres were further matured to form brain organoids in spinner flaks, in a medium composed of DMEM-F12: Neural Basal medium (1:1), 1:100 B27 v/o Vitamin A (Thermo Scientific), 1:200 N2 (Thermo Scientific), 1:100 L-Glutamine (Gibco), 100 µg/ml Primocin (Invitrogen), 0.05% Insulin (Sigma Aldrich) and 0.1% Matrigel (Corning).

**Infection of organoids**

60d old organoids with an estimated cell number of $2{,}5x10^6$ were maintained in organoid medium and preincubated with DMSO or 250 nM of 7.25 for 1h (final DMSO concentration was 0.5%). Then organoids were infected with HSV-1 at a moi of 0.1 or 1.0. At the next day the medium was renewed and new compound was added. After another 24h, the organoids were washed two times with PBS and then either fixed with 4% PFA at 4°C overnight (for ICC) or lysed with cold RIPA buffer (50 mM Tris-HCL, pH 7.4, 1% NP-40, 0.5% Na-deoxycholate, 0.1% SDS, 150 mM NaCl, 5 mM EDTA, 50 mM NaF) plus 1X Protease inhibitor cocktail and phosphatase inhibitor cocktail (Roche) followed by 4x sonication for 30s using a Misonix ultrasonic water bath at 100% amplitude. Protein concentration was determined with the DC Protein Assay (Bio-Rad).

**TUNEL assay**

Apoptotic cells were detected by TdT-mediated dUTP-biotin nick end labeling (TUNEL) using the DeadEnd Fluorometric TUNEL System (Promega, G3250) according to the manufacturers recommendations. At least three 10-µm sections of the brain organoids were analyzed by taking at least 10 images of each organoid. Dead cells were counted using ImageJ (NIH).

**Tau assay**

For the analysis of compound effects on tau phosphorylation $4x10^5$ SH-SY5Y tau-P301S cells were seeded on 24-well plates. At the next day the cells were treated with compounds diluted in DMSO. Final concentration of DMSO was 0.2%. After an incubation at 37°C, 5% $CO_2$ for 48h the cells were washed twice with PBS and then lysed in PBS/1% NP40 including the cOmplete protease inhibitor cocktail 2 (Roche) and phosphatase inhibitor cocktail (Roche). The protein concentration of the samples was determined with the DC Protein Assay (Bio-Rad) and 20 µg of each sample were separated on a NuPAGE 4-12% Bis-Tris gel and then transferred to a 0.2 µm membrane (Amersham) for Western Blot analysis.

***4. Cell lines***

**Generation of recombinant cell lines**

For the generation of a tau-P301S expression plasmid the multiple cloning site (MCS) of the pLHCX vector (Clontech) was modified by inserting a synthetic MCS-sequence (ACCGGTCTCGAGGCGGCCGCGGCCAAAAAGGCCGGATCCGTTAACACCAAAAA ATGGCACGTGGCCGGCACGCGTGGGCCCGTCGAC) between the HindIII and ClaI sites (pLHCX-mod-MCS). Then the ORF of human Tau 2N4R including the complete 3´-UTR was

ligated into pLHCX-mod-MCS via XhoI and BamHI. The P301S mutation was introduced by site-directed mutagenesis (CCG>TCG). Retroviruses were produced according to the manufacturer´s protocol (Clontech)

Human neuroblastoma SH-SY5Y cells were obtained mycoplasma-free from the DSMZ (Leibniz Institute DSMZ-German Collection of Microorganisms and Cell Cultures, Braunschweig, Germany) and tested at irregular time intervals for mycoplasma contamination. SH-SY5Y cells constitutively expressing human tau 2N4R-P301S were generated by retroviral infection of pLHCX-mod-MCS-tau-P301S according to the manufacturer´s protocol (Clontech)

For generation of the SH-SY5Y-tau-P301S MIF knockout line, we identified an sgRNA sequence specific for human MIF (exon 1) using the MIT-CRISPR server (http://crispr.mit.edu/): AGCTCGGAGAGGAACCCGTC. As negative control we used a scrambled sgRNA sequence: GCACTCACATCGCTACATCA (Applied Biological Materials, Richmond, BC, Canada). MIF-ko-5:CACCGAGCTCGGAGAGGAACCCGTC and MIF-ko-3: AAACGACGGGTTCCTCTCCGAGCTC as well as scrambled-5: CACCGGCACTCACATCGCTACATCA and scrambled-3: AAACTGATGTAGCGATGTGAGTGCC were phosphorylated with T4 PNK (Fermentas) in T4 ligation buffer (Fermentas). After annealing each set of oligonucleotides they were ligated into the lentiCRISPRv2 shuttle vector (Addgene, #52961) that was linearized with BsmBI (NEB) and dephosphorylated with FastAP (Fermentas). Finally, the product was transformed into Stbl3 bacteria. The cloning products were validated by sequencing. For further details, see the lentiCRISPRv2 and lentiGuide oligo cloning protocol provided by Addgene on the lentiCRISPRv2 website.

Lentiviral particles were produced in 90-100% confluent HEK293FT cells in a T75 flask. The cells were washed once with PBS before 5 mL Optimem (Invitrogen) were added 1h before transfection. The transfection mixture was prepared in 667 µL Optimem and contained 7 µg of the lentiviral shuttle vector as well as 4 µg pMDLG, 4 µg pRSV_Rev, and 4 µg pMD2.G for packaging. In another tube, 640 µL Optimem were supplemented with 27 µL Lipofectamine 2000 (ThermoFisher), and both mixtures were incubated for 5 min at RT. The DNA was then combined with the Lipofectamine-containing medium, followed by 20 min incubation at RT before it was added to the cells in a drop wise manner. After 14h the medium was changed to 6 mL of normal growth medium (DMEM). Following another 24h of incubation the cell culture supernatant containing the viral particles was passed through a sterile 0.45 µm filter to remove cell debris. Aliquots of 1 mL thereof were stored at -20°C.

For infection with lentiviral particles SH-SY5Y-tau-P301S cells were seeded into T25 flasks. At the next day the medium was replaced with 1 mL fresh complete growth medium and 10 µg polybrene (Sigma) as well as 1 mL of the viral particles were added to the cells. One flask was left uninfected for selection control and was provided with 2 mL polybrene-containing growth medium instead. After incubation for 24h the medium was removed and cells were washed twice with PBS. After adding 6 mL of fresh growth medium cells were incubated for another 24h. Then the cells were trypsinized resuspended in 10 mL growth medium containing 1 µg/mL of the selection marker puromycin and transferred to a new T75 flask. The medium was changed every 3-4 days and selection marker was added until stable cell clones appeared and non-infected control cells completely died. The knockout efficiency of MIF was analyzed by Western Blot.

**Culture and differentiation of LUHMES cells**

LUHMES cells (ATCC-CRL-2927) were maintained in a proliferative state in advanced DMEM/F12 (Gibco) supplemented with 1% N2 (ThermoFisher Scientific), 1% (v/v) penicillin/streptomycin (Invitrogen), 2 mM L-glutamine (Invitrogen) and 40 ng/mL bFGF (basic recombinant human fibroblast growth factor; Sigma) in flasks coated first with 50 µg/mL poly-L-ornithine (Sigma) and then with 1 µg/mL fibronectin (Sigma). For differentiation into post-mitotic neurons the cells were cultured in advanced DMEM/F12 supplemented with 1 µg/mL doxycycline (Sigma), 2 ng/mL GDNF (glial cell line-derived neurotropic factor; Sigma), and 1 mM dibutyryl-cAMP (Santa Cruz Biotechnology) in coated flasks for 2 days according to Scholz et al. (Scholz et al., 2011). The cells were then counted and seeded on target plates in differentiation medium.

**Neuronal differentiation and culture of IPSC**

iPSC culture and differentiation were performed as previously described, and all reagents were purchased from Thermo Fisher Scientific unless otherwise stated (Arber et al., 2020). iPSC were cultured on geltrex coated plates in Essential-8 media. iPSC were grown to 100% confluency prior to neuronal induction using dual SMAD inhibition as described previously (Shi et al., 2012). Briefly, cells were cultured for 10 days in neural induction media (N2B27 containing 10 µM SB431542 (Tocris) and 1 µM dorsomorphin (Tocris)). N2B27 media consists of a 1:1 mixture of Dulbecco's modified eagle medium F12 (DMEM-F12) and Neurobasal, supplemented with 1 × N-2, 1 × B-27, 5 µg/mL insulin, 1 mM l-glutamine, 100 µM nonessential amino acids, 100 µM 2-mercaptoethanol, 50 U ml−1 penicillin and 50 mg/mL streptomycin. At days 10 and 18, neuronal rosettes were passaged using dispase and plated in laminin-coated wells (Sigma L2020) in N2B27 media. The final passage was performed at day 35 using accutase, and cells were plated at a final density of 50,000 cells

per $cm^2$ and maintained in N2B27 media until treatment. Mature neurons were treated at 70-90 DIV and harvested 24-48h post-treatment.

**MTT assay**

For viability analysis $4x10^4$ Vero or $8x10^4$ SH-SY5Y-tau P301S cells were plated in a 96-well plate and incubated at 37°C, 5% $CO_2$ overnight. Then the compounds diluted in DMSO were added to the cells. The final concentration of DMSO was 1%. The cells were then incubated for 24h (Vero) or 48h (SH-SY5Y). Afterwards 20 µL of a Thiazolyl Blue Tetrazolium Bromide (MTT) solution (5 mg/mL in PBS) was added to the cells and incubated for 4h allowing viable cells to reduce the yellow MTT into blue formazan metabolites. Following aspiration of the medium, the formazan was resuspended in 200 µL isopropanol/ 40 mM HCl and incubated for 30 min at RT. The diluted formazan was spectrometrically analyzed at 560 nm and background at 670 nm was substracted.

**Immunocytochemistry**

For immunocytochemistry analysis $5x10^4$ LUHMES cells at differentiation day 2 were seeded on 13 mm coverslips that were coated with L-ornithine and fibronectine (see above) and placed into 24-well plates. After four additional days of differentiation the cells were infected with HSV-1 (moi =1). After 24h the cells were carefully washed with PBS and then fixed with PBS/4% PFA for 15 min at RT. The fixed cells were then permeabilized and blocked with 1%BSA (Sigma) /0.5% saponin (Sigma) and 5% (w/v) nonfat milk (Oxoid) for 1h at RT. Anti-HSV-1 gC diluted 1:500 in 1%BSA/0.5% saponin was applied overnight at 4°C. At the next day the cells were washed three times with PBS and then incubated with anti-mouse Alexa-fluor 488 (Invitrogen) for 1h at RT. Following washing three times with PBS and two times with water, cells were mounted with ProLong Gold with DAPI (Invitrogen), and imaged with a Zeiss Axiovision Apotome.2 microscope.

***5. Drug affinity chromatography (DRAC) and proteomics***

Pigs were raised in the Struve Lab, Manning, Iowa with proper food and free movement as per their IACUC protocol. They were euthanized and brains were removed immediately and homogenized in PBB containing 10 mM HEPES, 10 mM NaCl, 1 mM Mg, and 0.35% TX-100. 10% human brain homogenates were prepared in cold PBB and aliquots were flash frozen in liquid $N_2$. Homogenates were centrifuged at 10,000g for 10 min and supernatants were collected.

Cells were harvested by scraping into cold PBS and pelleted at 3,000g for 10 min at 4°C. The pellet was then resuspended in PBB yielding a concentration of approx. 5 mg/mL. The lysates were cleared by centrifugation and the supernatants were flash frozen.

For drug affinity chromatography, lysates or brain extracts were supplemented with 1 mM of ribonucleoside triphosphates (ATP, GTP, CTP, UTP), 10 mM creatine phosphate and 10 µL/mL of a 5 mg/mL stock solution of creatine kinase. The samples were then loaded onto 1.32 resin, equilibrated with PBB-buffer (plus supplements). After one hour of incubation at 26°C, the beads were washed with PBB (100x bed volume). Bound proteins were then eluted either with 200 µM 1.32 (pig brain) or 100 µM 7.25 (human brain samples) in the same buffer used as competitor solution or urea (cell lysates) for 1 hr. All elutions were kept frozen until further analysis.

For Mass spectrometric identification, pig brain eluates were run on a freshly prepared 12% SDS gel made up with all filtered solutions and chemicals to avoid Keratin contamination. Proteins bands were separated by gel electrophoresis at 100 V, constant for 1.5h. The marker and protein bands were fixed and stained with freshly prepared Coomassie blue (G250). All stains and destains were carried out with filtered solutions and all operation was done in a laminar flow hood again to avoid keratin contamination. Each stained band (as visualized under a white light box) was sliced (1 $mm^3$ per well (in 96 well MS/MS reaction plate (Intavis AG) in duplicates and sent out to USDA lab, Richmond, CA for further analysis. They were digested and analyzed by mass spectrometry (With Scaffold-2 viewer).

### *6. Recombinant MIF expression and NMR spectrometry*

**Generation of MIF expression constructs**

The open reading frame of human MIF was amplified by PCR from the vector pCMV6-entry MIF (Origene) and cloned into the pET11a vector (Novagen) via NdeI/BamHI using the following oligonucleotides: 5´-forward: aaaaaacatatgccgatgttcatcgtaaac and 3´-reverse:aaaaaaggatccttaggcgaaggtggag, allowing the tag-free expression in *E.coli*.

**Expression and purification of recombinant MIF**

For expression of $C^{13}/N^{15}$ labeled recombinant human wildtype-MIF BL21-(DE3)-Rosetta-pLysS bacteria (Novagen) were transformed with pET11a-MIF and spread on LB-Agar plates containing 50 µg/mL carbenicillin and 34 µg/mL chloramphenicol. One colony was used to inoculate a preculture of 10 ml M9 medium (plus $C^{13}$-labeled glucose and selection marker)

overnight at 37°C. At the next day 2 x 500 mL M9 medium containing $^{15}$N-labeled $NH_4Cl$ and $^{13}$C labeled glucose were inoculated with the preculture. The bacteria were grown to an $OD_{600}$ of 0.9 at 37°C before expression of MIF was induced by adding 1 mM IPTG (isopropyl b-D-thiogalactopyranoside). The protein was expressed overnight at 18°C. At the next day the bacteria were harvested by centrifugation, resuspended in 20 mM Tris-HCl pH7.5 and lysed by adding 20 mM $MgSO_4$, 20 U/mL DNaseI, and 100 µg/mL lysozyme for 30 min at RT. The lysate was cleared by centrifugation at 20,000g for 30 min and filtered through a 0.45 µm cellulose acetate membrane (VWR). In order to purify MIF the lysate was first passed over a 5-mL CM-sepharose column (GE Healthcare), and after washing with 10 column volumes (CV) of 20 mM Tris-HCl pH7.5 MIF was eluted with 20 mM Tris pH7.5, 100 mM NaCl. The eluate was then diluted 3x with 20 mM Tris-HCl pH7.5 and passed over a 5 mL Q-sepharose column (GE Healthcare). The Flow through containing the MIF protein was then again loaded on a 5 mL CM sepharose column. The column was washed with 10 CV 20 mM sodium phosphate buffer (NaPi) pH 7.2 and then MIF was eluted with NaPi pH7.2, 100 mM NaCl. The purity of MIF was validated by SDS-PAGE and aliquots were stored at -80°C.

**NMR structure**

The NMR $F_1$-[$^{13}$C,$^{15}$N]-filtered-[$^{1}$H,$^{1}$H]-NOESY spectra for structure calculation were recorded on a 700 MHz Bruker Avance Neo spectrometer equipped with cryoprobe, and the $^{15}$N-HSQC were recorded on a 600 MHz Bruker Avance III spectrometer equipped with cryoprobe. The filtered NOESY were recorded at 310K to reduce the rotational correlation time of the system, with two different mixing times 60 and 100ms; the free induction decay was measured for 106ms (2048 points) and the indirect dimension was set to 20ms (400 points); the signal acquisition was performed with 160 scans and the interscan delay was set to 1.5s. The $^{15}$N-HSQC were measured at 298K with 121ms (2048 points) in the direct dimension and 53ms (256 points) in the indirect dimension; the signal acquisition was performed through the accumulation of 16 scans and an interscan delay of 1s was applied.

**SEC-HPLC-MALS**

The samples for SEC-HPLC-MALS were 100 uM of MIF (WT or mutant C81W) in 20 mM phosphate buffer, with or without compound 7.25 (100 uM).

The HPLC-MALS was perform at 0.5 mL/min and 25°C with an Agilent 1200 series HPLC system and a size exclusion column TSKgel G2000SWXL from Tosoh bioscience. The detection was performed recording the UV absorbance at 280 nm with the HPLC detector and the light scattering with a miniDawn Treos spectrometer from Wyatt. The molecular weight of the detected species is calculated using the extinction coefficients at 280 nm

(12950 $M^{-1}$ $cm^{-1}$ for WT and 18450 $M^{-1}$ $cm^{-1}$ for C81W), absorbance at 280 nm and the Rayleigh ratio using the built-in function in Astra software.

### *7. Immunoassays*

**Primary antibodies:**

Rabbit anti-HSV1 polyclonal – abcam ab9533 (WB: 1:500)

Mouse anti-HSV1 gC [3G9] monoclonal – abcam ab6509 (InCell ELISA: 1:10,000; ICC: 1:500; WB: 1:2,000)

Mouse anti GAPDH [A-3] monoclonal – Santa Cruz Biotechnology (WB: 1:200)

Rabbit anti TUJ-1 polyclonal - Sigma T2200 (ICC: 1:400)

Mouse anti tau (total) HT7 – Thermofisher – MN1000 (WB: 1:1,000)

Mouse anti phospho-tau (Ser202, Thr205) AT8 – Thermofisher – MN1020 (WB: 1:1,000)

Mouse anti phospho-tau (Thr231) AT180 – Thermofisher – MN1040 (WB: 1:1,000)

Mouse anti phospho-tau (Thr181) AT270– Thermofisher – MN1050 (WB: 1:1,000)

Mouse anti phospho-tau (Ser396/ Ser404) – PHF-1 (provided by Dr. Peter Davies) (WB: 1:5,000)

Rabbit anti-MIF – Sigma – HPA 003868 (WB: 1:1000)

Mouse anti-MIF(10C3) – Biolegend #525501 (ELISA: 0.5µg/well)

Human anti-oxMIF (Imalumab) – Creative Biolabs (ELISA: 1:2000)

Rabbit anti-cutA – Sigma – HPA 064369 (WB: 1:1000)

**Secondary antibodies:**

Goat anti-human IgG-HRP, Southern Biotech - #2087-05 (ELISA: 1:5,000)

Goat anti-Mouse IgG - IRDye 800CW, LI-COR Biosciences - 925-32210 (WB: 1:20,000)

Goat anti-Rabbit IgG - IRDye 800CW, LI-COR Biosciences - 925-32211 (WB: 1:20,000)

Goat anti-Mouse IgG - IRDye 680RD, LI-COR Biosciences - 926-68070 (WB: 1:20,000)

Goat anti-Rabbit IgG - IRDye 680RD, LI-COR Biosciences - 926-68071 (WB: 1:20,000)

Goat anti-mouse IgG-Alexa-fluor 488, Invitrogen (ICC: 1:1,000)

Donkey anti-rabbit Alexa Fluor 647 – Thermo Scientific A28175 (ICC: 1:500)

**Immunoblot**

After the protein concentration of cell lysates and homogenates had been determined using the DC Protein Assay Kit (Bio-Rad) 20 µg of each sample were dissolved in NuPAGE LDS Sample buffer (including 2% β-mercaptoethanol), boiled at 100°C for 5 min and then separated on NuPAGE Novex 4-12% Bis-Tris midi gels (Invitrogen) using NuPAGE MES

SDS Running buffer (Invitrogen). Proteins were then transferred to a 0.2 µm nitrocellulose membrane (Amersham) in Tris/glycine/ 20% MeOH at 400 mA for 2h using a tank blot system (Bio-Rad). In order to detect any blotting artifacts the proteins on the membranes were visualized with Ponceau red solution. The membranes were destained with PBS and then blocked with PBS/ 5% nonfat milk (Oxoid) for 1h at RT. Incubations with primary antibodies diluted in PBS-T were carried out overnight at 4°C. Then the membranes were washed three times with PBS-T for 10 min and afterwards incubated with fluorescent secondary antibodies (IR Dye 680 or 800: Li-COR Biosciences.) diluted 1:20,000 in PBS-T for 1h at RT. Following three washing steps with PBS-T for 10 min each, the membranes were scanned using the LI-COR Odyssey CLX. Signal intensities were calculated using the Image Studio Version 2.1 software (LI-COR Biosciences).

**Sandwich ELISA**

For quantitative determination of oxidized MIF (oxMIF), 96-well-Immuno Maxisorp plates (Nunc) were coated with 0.5 µg/ well of 10C3 in 50 mM carbonate buffer pH 9.4 to capture total MIF species. The wells were blocked with PBS/5% BSA/ 0.1% Tween-20 for 2h at RT. After washing with PBS-T, samples diluted in PBS/1% BSA/ 0.1% Tween-20 were added and incubated overnight at 4°C. The wells were washed 3x with PBS-T and incubated with the oxMIF specific antibody Imalumab at a 1:2,000 dilution for 4h at RT. Then, the wells were again washed 3x with PBST before a goat anti-human IgG-HrP conjugate (1:5,000 dilution) was added for 1h at RT. After 4x washing with PBS-T the ELISA was developed with 1-step Ultra TMB ELISA (Thermo Scientific). For generation of an oxMIF standard curve, recombinant wt-MIF was treated with 0.2% Proclin300 that transforms recombinant MIF into an oxMIF surrogate as described in (Thiele et al., 2015).

### *8. Statistics*

All statistical analyses were performed as indicated using GraphPad Prism (Versions 6; GraphPad Software Inc., San Diego, CA, USA). Appropriate statistical tests and p-values are stated in the respective figure legends. p-values of *$p \leq 0.05$, **$p \leq 0.01$, ***$p \leq 0.001$, ****$p \leq 0.0001$ were used as significance levels.

### *9. Ethics statement*

Human brain samples were obtained from the The Netherlands Brain Bank, Netherlands Institute for Neuroscience, Amsterdam (www.brainbank.nl). Use of these samples for this study was approved by the Ethics Commission of the Medical Faculty of the Heinrich Heine University, Düsseldorf.

**Acknowledgements**

This research was funded by BMBF REMOVAGE (#01GQ1422A), the Research Commission of the Medical Faculty of the Heinrich Heine University Düsseldorf (#9772726), the DFG (KO1679/10-1, 15-1), and a grant from Prosetta Biosciences.

**References**

Allnutt, M.A., Johnson, K., Bennett, D.A., Connor, S.M., Troncoso, J.C., Pletnikova, O., Albert, M.S., Resnick, S.M., Scholz, S.W., De Jager, P.L.*, et al.* (2020). Human Herpesvirus 6 Detection in Alzheimer's Disease Cases and Controls across Multiple Cohorts. Neuron *105*, 1027-+.

Arber, C., Toombs, J., Lovejoy , C., Ryan, N.S., Paterson, R.W., Willumsen, N., Gkanatsiou, E., Portelius, E., Blennow, K., Heslegrave, A.*, et al.* (2020). Familial Alzheimer's disease patient-derived neurons reveal distinct mutation-specific effects on amyloid beta. . Molecular Psychiatry *25*, 2919-2931.

Augustinack, J., Schneider, A., Mandelkow , E.M., and Hyman, B.T. (2002). Specific tau phosphorylation sites correlate with severity of neuronal cytopathology in Alzheimer's disease. Acta Neuropathol *103*, 26-35.

Bacher, M., Deuster, O., Aljabari, B., Egensperger, R., Neff, F., Jessen, F., Popp, J., Noelker, C., Reese, J.P., Al-Abed, Y.*, et al.* (2010). The role of macrophage migration inhibitory factor in Alzheimer's disease. Mol Med *16*, 116-121.

Bonham, L.W., Karch, C.M., Fan, C.C., Tan, C., Geier, E., Wang, Y., Wen, N., Broce, I.J., Li, Y., Barkovich, M.J.*, et al.* (2018). CXCR4 involvement in neurodegenerative diseases. Translational Psychiatry *11*, 73.

Chen, H., He, Y., Ji, J., and Shi, Y. (2019). A Machine Learning Method for Identifying Critical Interactions Between Gene Pairs in Alzheimer's Disease Prediction. Frontiers in Neurology *10*, 1162.

Cirone, M. (2018). EBV and KSHV Infection Dysregulates Autophagy to Optimize Viral Replication, Prevent Immune Recognition and Promote Tumorigenesis. Viruses *10*.

Eimer, W.A., Vijaya Kumar, D.K., Navalpur Shanmugam, N.K., Rodriguez, A.S., Mitchell, T., Washicosky, K.J., Gyorgy, B., Breakefield, X.O., Tanzi, R.E., and Moir, R.D. (2018). Alzheimer's Disease-Associated beta-Amyloid Is Rapidly Seeded by Herpesviridae to Protect against Brain Infection. Neuron *99*, 56-63 e53.

Fabiani, M., Limongi, D., Palamara, A., De Chiara, G., and Marcocci, M. (2017). A Novel Method to Titrate Herpes Simplex Virus-1 (HSV-1) Using Laser-Based Scanning of Near-Infrared Fluorophores Conjugated Antibodies. Frontiers in Microbiology *8*, 1085.

Gabriel, E., Ramani, A., Karow, U., Gottardo, M., Natarajan, K., Gooi, L.M., Goranci-Buzhala, G., Krut, O., Peters, F., Nikolic, M.*, et al.* (2017). Recent Zika Virus Isolates Induce Premature Differentiation of Neural Progenitors in Human Brain Organoids. . Cell Stem Cell *20*, 397-406.e395.

Hou P, Liu G, Zhao Y, Shi Z, Zheng Q, Bu G, Xu H, and YW, Z. (2015). Role of copper and the copper-related protein CUTA in mediating APP processing and Aβ generation. . Neurobiology of Aging *36*, 1310-1315.

Itzhaki, R.F., Golde, T.E., Heneka, M.T., and Readhead, B. (2020). Do infections have a role in the pathogenesis of Alzheimer disease? Nat Rev Neurol.

Itzhaki, R.F., Lin, W.R., Shang, D.H., Wilcock, G.K., Faragher, B., and Jamieson, G.A. (1997). Herpes simplex virus type 1 in brain and risk of Alzheimer's disease. Lancet *349*, 241-244.

Jankauskas, S.S., Wong, D.W.L., Bucala, R., Djudjaj, S., and Boor, P. (2019). Evolving complexity of MIF signaling. . Cellular Signaling *57*, 76-88.

Jeffery, C.J. (2020). Enzymes, pseudoenzymes, and moonlighting proteins: diversity of function in protein superfamilies. FEBS J.

Kassaar, O., Pereira Morais, M., Xu, S., Adam, E.L., Chamberlain, R.C., Jenkins, B., James, T.D., Francis, P.T., Ward, S., Williams, R.J.*, et al.* (2017). Macrophage Migration Inhibitory Factor is subjected to glucose modification and oxidation in Alzheimer's Disease. Sci Rep *7*, 42874.

Li, S.Q., Yu, Y., Han, J.Z., Wang, D., Liu, J., Qian, F., Fan, G.H., Bucala, R., and Ye, R.D. (2015). Deficiency of macrophage migration inhibitory factor attenuates tau hyperphosphorylation in mouse models of Alzheimer's disease. J Neuroinflammation *12*, 177.

Lingappa, U.F., Wu, X., Macieik, A., Yu, S.F., Atuegbu, A., Corpuz, M., Francis, J., Nichols, C., Calayag, A., Shi, H.*, et al.* (2013a). Host-rabies virus protein-protein interactions as druggable antiviral targets. Proc Natl Acad Sci U S A *110*, E861-868.

Lingappa, V., Harrell, E., Copeland, K., Prasad, M.D., Asundi, V., Hahner, N., Francis, J., Dey, D., Welsh, J.C., Macieik, A.*, et al.* (2010). Cell-Free Protein Synthesizing Systems As Tools for Discovery of Drugs Inhibiting Viral Capsid Assembly. Antiviral Res. 2010; 86 (1) pA61.

Lingappa, V.R., Hurt, C.R., and Garvey, E. (2013b). Capsid assembly as a point of intervention for novel anti-viral therapeutics. Curr Pharm Biotechnol *14*, 513-523.

Lovheim, H., Gilthorpe, J., Adolfsson, R., Nilsson, L.G., and Elgh, F. (2015). Reactivated herpes simplex infection increases the risk of Alzheimer's disease. Alzheimers Dement *11*, 593-599.

Marreiros, R., Muller-Schiffmann, A., Trossbach, S.V., Prikulis, I., Hansch, S., Weidtkamp-Peters, S., Moreira, A.R., Sahu, S., Soloviev, I., Selvarajah, S.*, et al.* (2020). Disruption of cellular proteostasis by H1N1 influenza A virus causes alpha-synuclein aggregation. Proc Natl Acad Sci U S A *117*, 6741-6751.

Martinez-Martin, N., Viejo-Borbolla, A., Martín, R., Blanco, S., Benovic, J.L., Thelen , M., and Alcamí, A. (2015). Herpes simplex virus enhances chemokine function through modulation of receptor trafficking and oligomerization. Nat Commun. 2015 Jan 27;6:6163. doi: 10.1038/ncomms7163. PMID: 25625471.

Müller-Schiffmann, A., Trossbach, S.V., Lingappa, V.R., and Korth, C. (2020). Viruses as 'Truffle Hounds': Molecular Tools for Untangling Brain Cellular Pathology. Trends in Neurosciences *S0166-2236*.

Nasiri, E., Sankowski, R., Dietrich, H., Oikonomidi, A., Huerta, P.T., Popp, J., Al-Abed, Y., and Bacher, M. (2020). Key role of MIF-related neuroinflammation in neurodegeneration and cognitive impairment in Alzheimer's disease. . Molecular Medicine *26*, 34.

Orvedahl, A., Alexander, D., Talloczy, Z., Sun, Q., Wei, Y., Zhang, W., Burns, D., Leib, D.A., and Levine, B. (2007). HSV-1 ICP34.5 confers neurovirulence by targeting the Beclin 1 autophagy protein. Cell Host Microbe *1*, 23-35.

Petralia, M.C., Battaglia, G., Bruno, V., Pennisi, M., Mangano, K., Lombardo, S.D., Fagone, P., Cavalli, E., Saraceno, A., Nicoletti, F.*, et al.* (2020). The Role of Macrophage Migration Inhibitory Factor in Alzheimer's Disease: Conventionally Pathogenetic or Unconventionally Protective? Molecules *25*.

Rajasekaran, D., Gröning, S., Schmitz, C., Zierow, S., Drucker, N., Bakou, M., Kohl, K., Mertens, A., Lue, H., Weber, C.*, et al.* (2016). Macrophage Migration Inhibitory Factor-CXCR4 Receptor Interactions: EVIDENCE FOR PARTIAL ALLOSTERIC AGONISM IN COMPARISON WITH CXCL12 CHEMOKINE. Journal of Biological Chemistry *291*, 15881-15895.

Readhead, B., Haure-Mirande, J.V., Funk, C.C., Richards, M.A., Shannon, P., Haroutunian, V., Sano, M., Liang, W.S., Beckmann, N.D., Price, N.D.*, et al.* (2018). Multiscale Analysis of Independent Alzheimer's Cohorts Finds Disruption of Molecular, Genetic, and Clinical Networks by Human Herpesvirus. Neuron *99*, 64-82 e67.

Reed, J.C., Solas, D., Kitaygorodskyy, A., Freeman, B., Ressler, D.T.B., Phuong, D.J., Swain, J.V., Matlack, K., Hurt, C.R., Lingappa, V.R.*, et al.* (2021). Identification of an Antiretroviral Small Molecule That Appears To Be a Host-Targeting Inhibitor of HIV-1 Assembly. J Virol *95*(3):e00883-20

Schinagl, A., Kerschbaumer, R.J., Sabarth, N., Douillard, P., Scholz, P., Voelkel, D., Hollerweger, J.C., Goettig, P., Brandstetter, H., Scheiflinger, F.*, et al.* (2018). Role of the Cysteine 81 Residue of Macrophage Migration Inhibitory Factor as a Molecular Redox Switch. Biochemistry *57*, 1523-1532.

Scholz, D., Pöltl, D., Genewsky, A., Weng, M., Waldmann, T., Schildknecht, S., and Leist, M. (2011). Rapid, complete and large-scale generation of post-mitotic neurons from the human LUHMES cell line. Journal of neurochemistry *119*, 957-971.

Selvarajah, S., Lingappa, A.F., Michon, M., Yu, S.F., Macieik, A., Mallesh, S., Appaiah, U., Crabtree, J., Copeland, K., Lin, J.*, et al.* (2021). From COVID-19 to the Common Cold: Novel Host-Targeted, Pan-Respiratory Antiviral Small Molecule Therapeutics. bioRxiv, 2021.2001.2017.426875.

Shi, Y., Kirwan , P., and Livesey, F.J. (2012). Directed differentiation of human pluripotent stem cells to cerebral cortex neurons and neural networks. Nature Protocols *7*, 1836-1846.
Szeliga, M. (2020). Peroxiredoxins in Neurodegenerative Diseases. Antioxidants *9*, 1203.

Thiele, M., Kerschbaumer, R.J., Tam, F.W., Volkel, D., Douillard, P., Schinagl, A., Kuhnel, H., Smith, J., McDaid, J.P., Bhangal, G.*, et al.* (2015). Selective Targeting of a Disease-Related Conformational Isoform of Macrophage Migration Inhibitory Factor Ameliorates Inflammatory Conditions. J Immunol *195*, 2343-2352.

Tzeng, N.S., Chung, C.H., Lin, F.H., Chiang, C.P., Yeh, C.B., Huang, S.Y., Lu, R.B., Chang, H.A., Kao, Y.C., Yeh, H.W.*, et al.* (2018). Anti-herpetic Medications and Reduced Risk of Dementia in Patients with Herpes Simplex Virus Infections-a Nationwide, Population-Based Cohort Study in Taiwan. Neurotherapeutics *15*, 417-429.

Wang, T. (2015). Glutathione S-transferases variants as risk factors in Alzheimer's disease. . Neurological Science *36*, 1785-1792.

Wozniak, M.A., Frost, A.L., and Itzhaki, R.F. (2009). Alzheimer's Disease-Specific Tau Phosphorylation is Induced by Herpes Simplex Virus Type 1. J Alzheimers Dis *16*, 341-350.

## Figure legends

### Figure 1. Drug targeting host proteins (7.25) prevents HSV-1 infection in differentiated LUHMES and human brain organoids

**A** The antiviral activity of 7.25 was determined by standard plaque assay displaying infective viral units from the lysates of infected Vero cells (moi = 1) that were treated with 7.25 between 6 nM and 200 nM. Each data point displays the mean +/- SEM of three experiments (n=3). The $IC_{50}$ of 7.25 was calculated to be 32 nM.

**B** The results were validated by an in-Cell ELISA, measuring HSV-1gC in Vero cells treated with increasing concentrations of 7.25 and infected with HSV-1 (moi = 1). Each data point displays the mean +/- SEM of three independent experiments (n=3). Here, the $IC_{50}$of 7.25 was calculated to be 25 nM.

**C** ICC of differentiated LUHMES cells infected with HSV-1 (moi = 1) for 24h either treated with DMSO or 50 nM of 7.25. The cells were stained with a polyclonal antibody against HSV-1 (ab9533; green). Cell nuclei were stained with DAPI. Viral antigens were detected within the nucleus and cytoplasm as well as in the axons of non-treated cells. 7.25 markedly reduced the presence of viral antigens. Only within the nucleus signals could be detected. (bar = 10 µm)

**D** Western Blot of cell lysates derived from differentiated LUHMES cells that were infected with increasing mois of HSV-1 (0.05 to 1.0) and treated with DMSO or 50 nM of 7.25. The upper signal represents a HSV-1 antigen detected with ab9533. GAPDH was used as internal control. The diagram below shows the HSV-1 signals normalized to GAPDH from three (n=3) independent experiments. Data are presented as mean +/- SEM. One-way ANOVA (Holm-Sidak post-hoc) *p<0.05; ***p<0.001

**E** Staining of 60d human brain organoids that were infected with HSV-1 (moi = 1) for 48h and treated with DMSO or 250 nM of 7.25. HSV-1 (green) infected TUJ-1-positive neurons (magenta) in the outer layer of the organoids. Infection with HSV-1 was completely abolished when 7.25 was present (lower panel). (bars = 30 µm)

**F** Western Blot with lysates from 60d human brain organoids infected with HSV-1 (moi of 0.1 or 1.0). HSV-1 signals were normalized with GAPDH. The diagram below represents the results from three infected organoids that were analyzed in three (n=3) independent Western Blots. Data are presented as mean +/- SEM. One-way ANOVA (Holm-Sidak post-hoc) ****p<0.0001

**G** 7.25 (250 nM) also lowered cell toxicity mediated by HSV-1 infection. Compared to the mock condition, HSV-1 infected organoids displayed increased TUNEL-positive cells, which was reverted by addition of 7.25. For each condition three different organoids (n=3) and at

least 10 images of every organoid were analyzed. Data are presented as mean +/- SEM. One-way ANOVA followed by Tukey´s multiple comparison test, *p<0.05

**Table 1.** Structure of synthesized compounds including $IC_{50}$ values derived by in-Cell ELISA

**Table 2.** List of peptides identified by DRAC analysis including Mascot ion score

**Figure 2. DRAC identifies macrophage migration inhibitory factor (MIF) as functional target of 7.25**

**A** Production of infectious particles was not changed in MIF-knockout cells but efficiency of 7.25 was reduced. Plaque assays were performed with lysates from SH-CRISPR-Control and SH-MIF-knockout cells that were either treated with DMSO or 7.25 (5 nM) and infected with HSV-1 (moi 0.2). The diagram shows the viral titers from eight (n=8) infections. Data are presented as mean +/- SEM. One-way ANOVA (Sidak´s post-hoc) **p<0.01.

**B** Knock out of MIF enhanced production of HSV-1 gene products SH- CRISPR -Control and SH-MIF-knockout cells were infected with increasing mois of HSV-1 (moi 0.05 to 0.8). In MIF-ko cells the production of viral proteins was fascilitated. The diagram shows the HSV-1 signals normalized to GAPDH from four (n=4) independent experiments. Data are presented as mean +/- SEM. One-way ANOVA (Holm-Sidak post-hoc) ****p<0.0001

**Figure 3. Structural features of the MIF-7.25 interaction**

**A**. Structure of the MIF trimer interface with the residues showing chemical shift perturbations in the HSQC spectra (Supplementary Figure 5B) represented in orange sticks. Each monomer is represented in a different color, i.e., cyan and grey. **B**, Structure of the compound 7.25 in complex with MIF calculated with the *N*MR$^2$ protocol using ligand to protein's aromatics and ligand to protein's methyls distance restraints. The 10 best calculated poses have been retained, i.e., the poses with the lowest target function.

**Figure 4. Increased presence of oxMIF in brain samples of AD patients**

**A**. DRAC analysis of 20 brain samples from AD patients and age-matched healthy controls. Left: WB (representative section); upper panel shows the loading control (MIF and GAPDH) from brain homogenates applied to 1.32 resin and the lower panel the pulled-down and 7.25-eluted MIF. The GAPDH normalized MIF protein levels within the brain samples did not significantly differ between AD and control (left diagram). The eluted MIF was normalized to

the input MIF/GAPDH signal (right diagram). Significantly more MIF was precipitated from AD brain samples by DRAC (displayed as % of the average in control samples). Each data point represents the average of two independent experiments. Data are presented as mean +/- SEM. Two tailed t-test *p<0.05

**B.** OxMIF in brain samples used for DRAC was detected by Sandwich ELISA. A significant higher oxMIF concentration (ng/mg protein) was detected in AD-brain tissue (upper and lower diagram) whereas the total MIF concentration as measured by quantitative Western Blot did not differ (middle diagram; Supplementary Figure 6D). The ratio of oxMIF/ total MIF is shown in the right diagram. Each data point represents the average of two independent brain sample preparations. Data are presented as mean +/- SEM. Two tailed t-test *p<0.05.

**C.** Correlation analysis of the 20 brain samples between oxMIF levels detected by sandwich ELISA and MIF species eluted from 1.32 resin. The oxMIF levels positively correlated with the amounts of MIF species eluted from 1.32 resin. Spearman´s rho coefficient and p value are indicated in the graph.

**Figure 5. Effects of 7.25 on tau phosphorylation and role of HSV-1 infection and MIF**

**A** Infection of SH-SY5Y-tau P301S cells with low moi of HSV-1 (0,03 and 0,1) increased tau phosphorylation (AT8) 6h post infection. This increase was absent in the presence of 7.25 (20 nM). The diagram shows the AT8 signals normalized to total tau (HT7) from five (n=5) independent experiments. Data are presented as mean +/- SEM. One-way ANOVA (Dunnett´s post-hoc) *p<0.05

**B** 7.25 dose dependently reduced tau phosphorylation at the AT8 site at low nanomolar concentrations also in the absence of viral infection. SH-SY5Y-tau P301S cells were treated with 7.25 for 48h. Already 10 nM of 7.25 were sufficient to significantly reduce tau phosphorylation. The values from four independent experiments (n=4) are presented as mean +/- SEM. One-way ANOVA (Dunnett´s post-hoc) *p<0.05

**C** SAR of 7.25 analogs on tau phosphorylation. SH-SY5Y-tau P301S cells were treated with 500 nM of 7.25 analogs for 48h. Lysates were then analyzed by Western blot. The diagram shows the AT8 signals normalized to total tau from four independent experiments (n=4). Data are presented as mean +/- SEM. One-way ANOVA (Dunnett´s post-hoc) *p<0.05

**D** Correlation analysis of the 7.25 analogs between reduction of tau phosphorylation (% of DMSO) and inhibition of HSV-1 activity ($IC_{50}$). The effects of the compounds on tau phosphorylation positively correlated to their capacity to inhibit HSV-1 replication. Spearman´s rho coefficient and p value are indicated in the graph.

**E** Reduction of tau phosphorylation (AT8) by 7.25 was impaired in SH-tauP301S-MIF-knockout cells. The diagram shows the average values of five independent experiments

(n=5). Data are presented as mean +/- SEM. One-way ANOVA (Dunnett´s post-hoc) **p<0.01; *p<0.05

**F** 7.25 reduced tau phosphorylation (PHF-1) in differentiated neurons derived from human iPSCs. The neurons were incubated with 7.25 (50 nM) for 48h. The diagram shows the average values of three independent experiments (n=3). Data are presented as mean +/- SEM. One-tailed t-test *p<0.05

# Figure 1

**Figure 2**

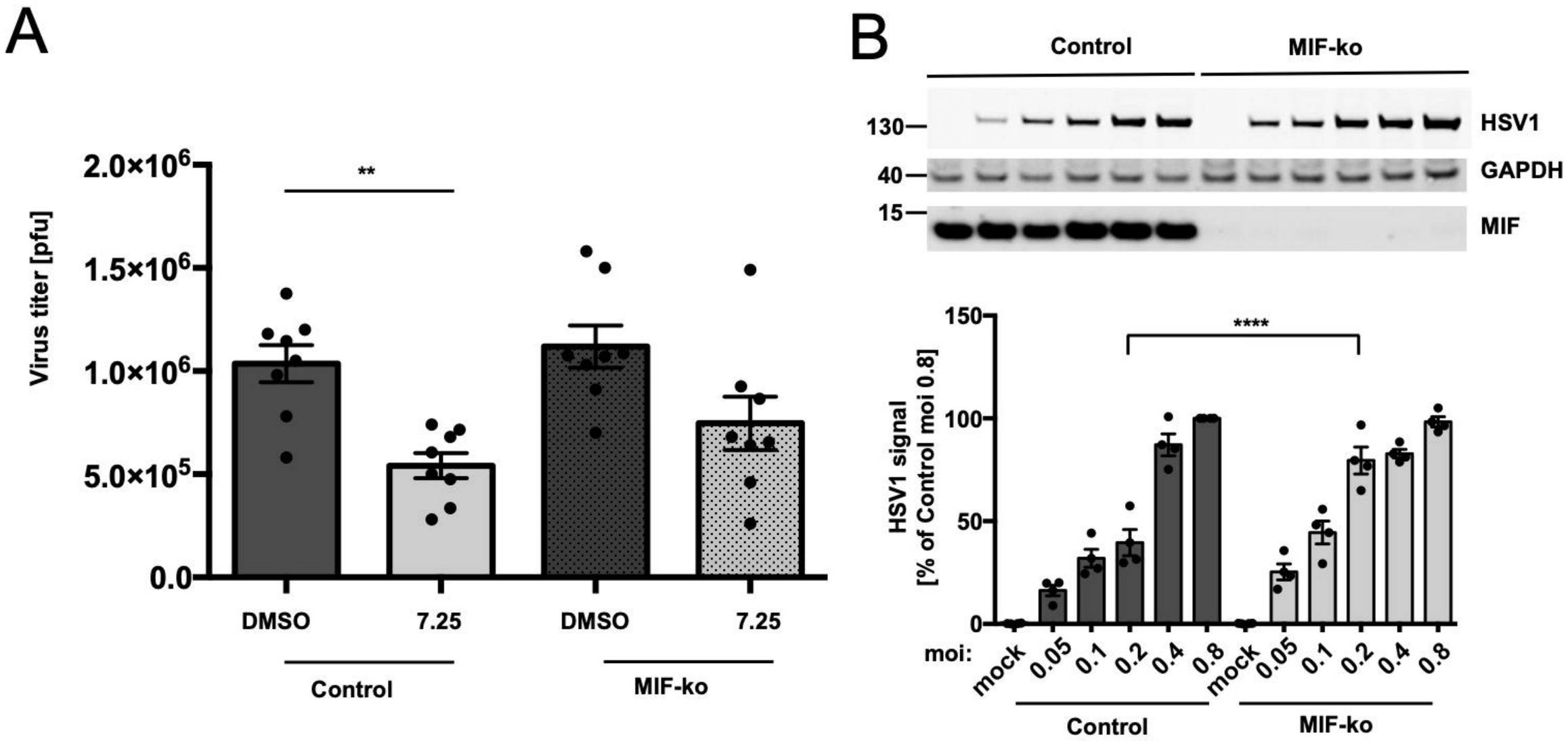

# Figure 3

A

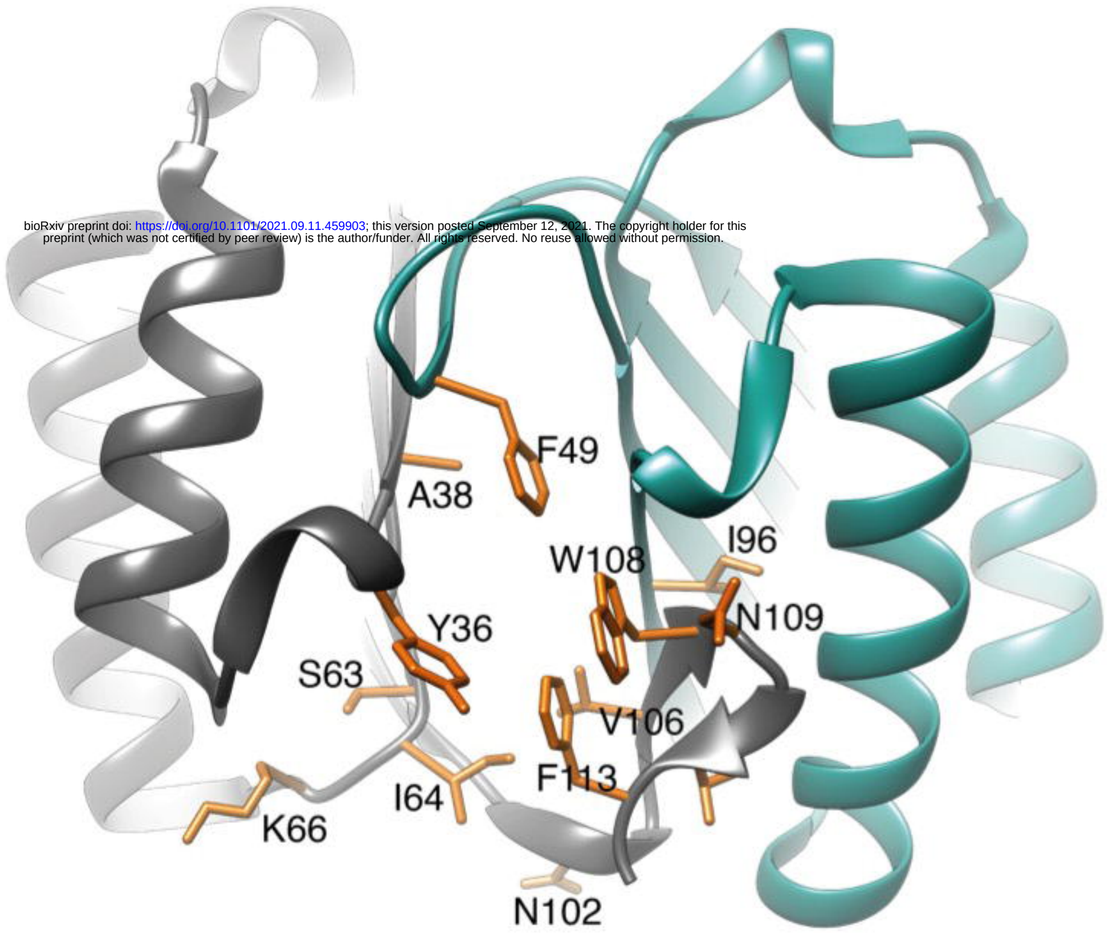




B

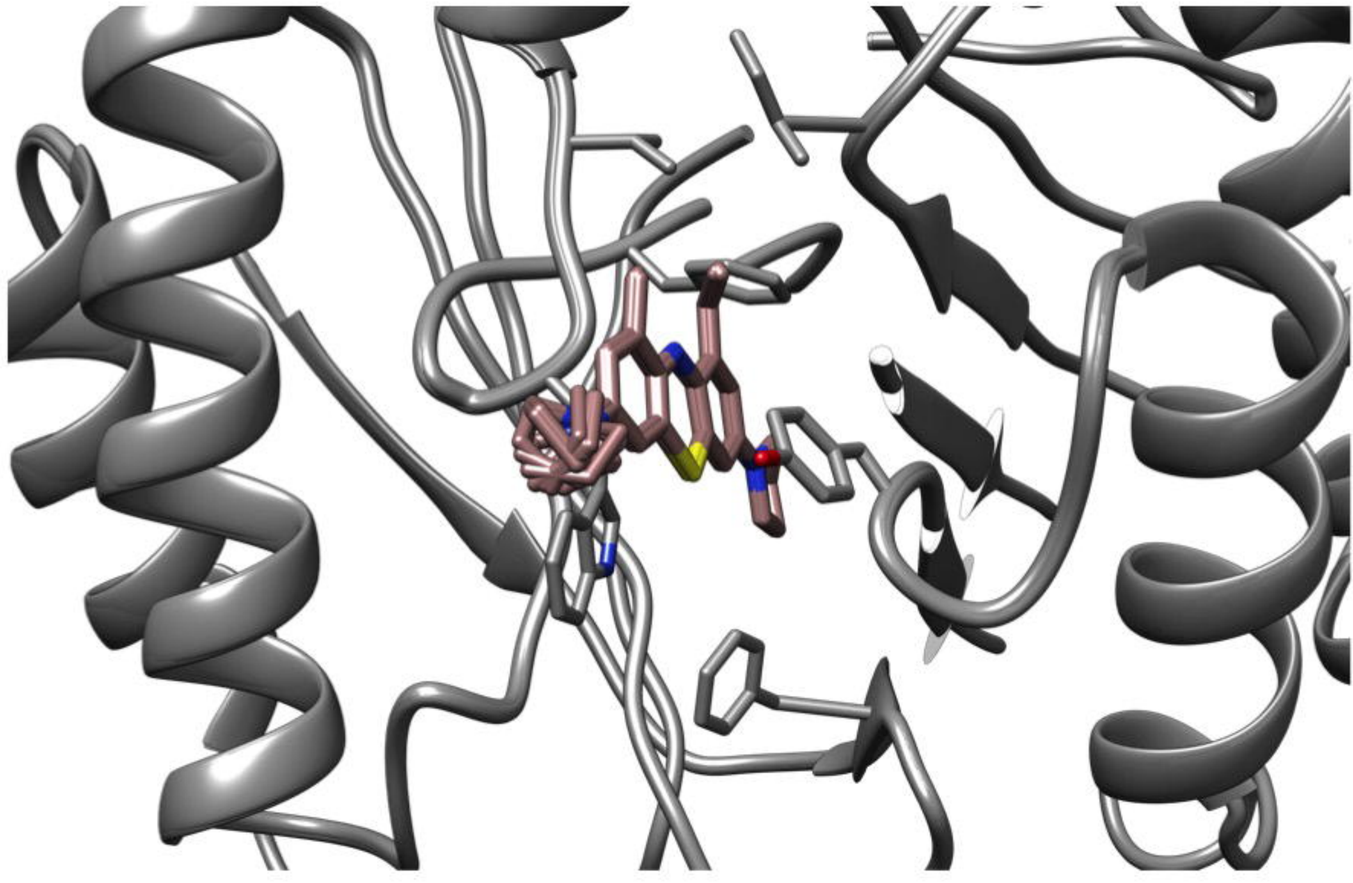

**Figure 4**

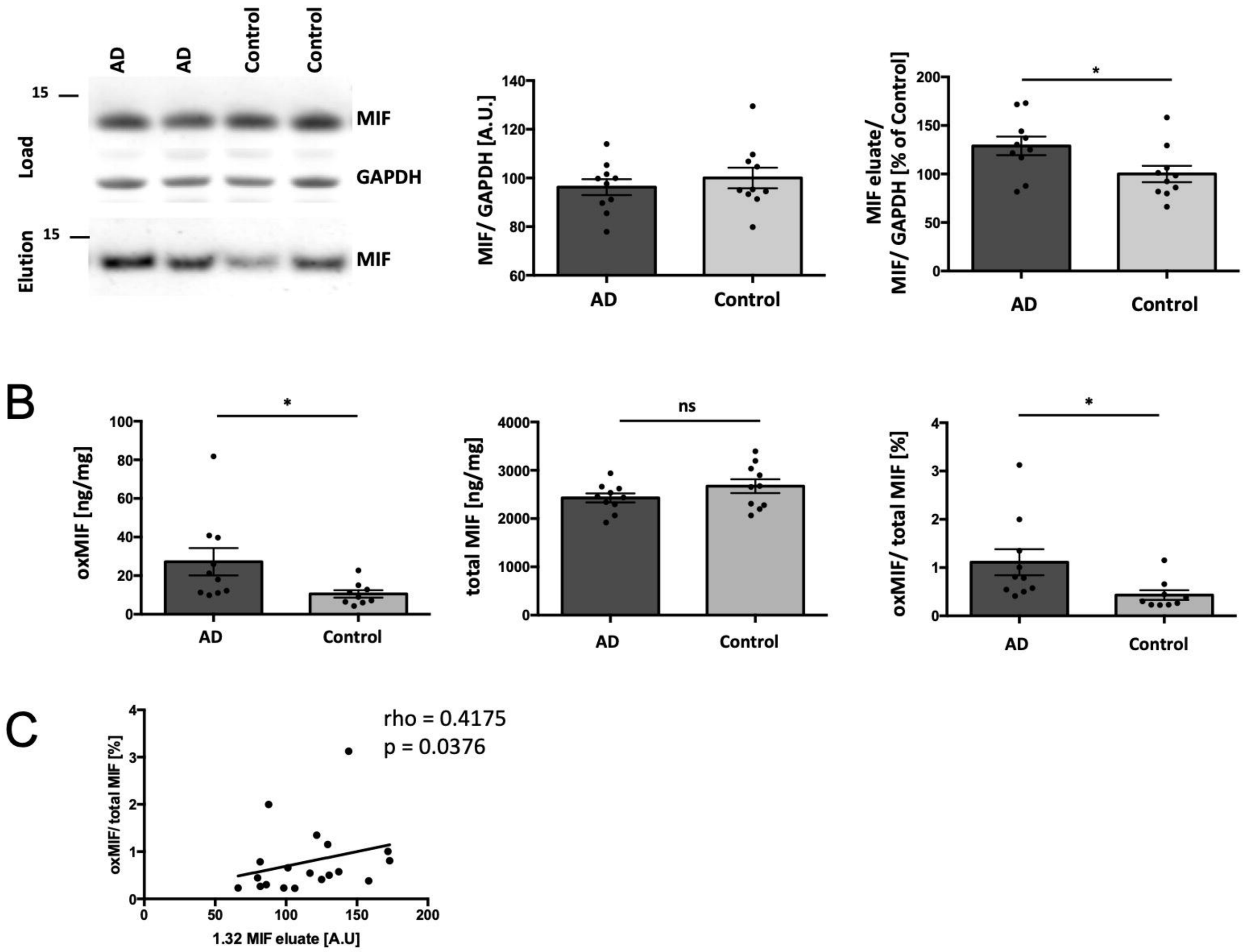

**Figure 5**

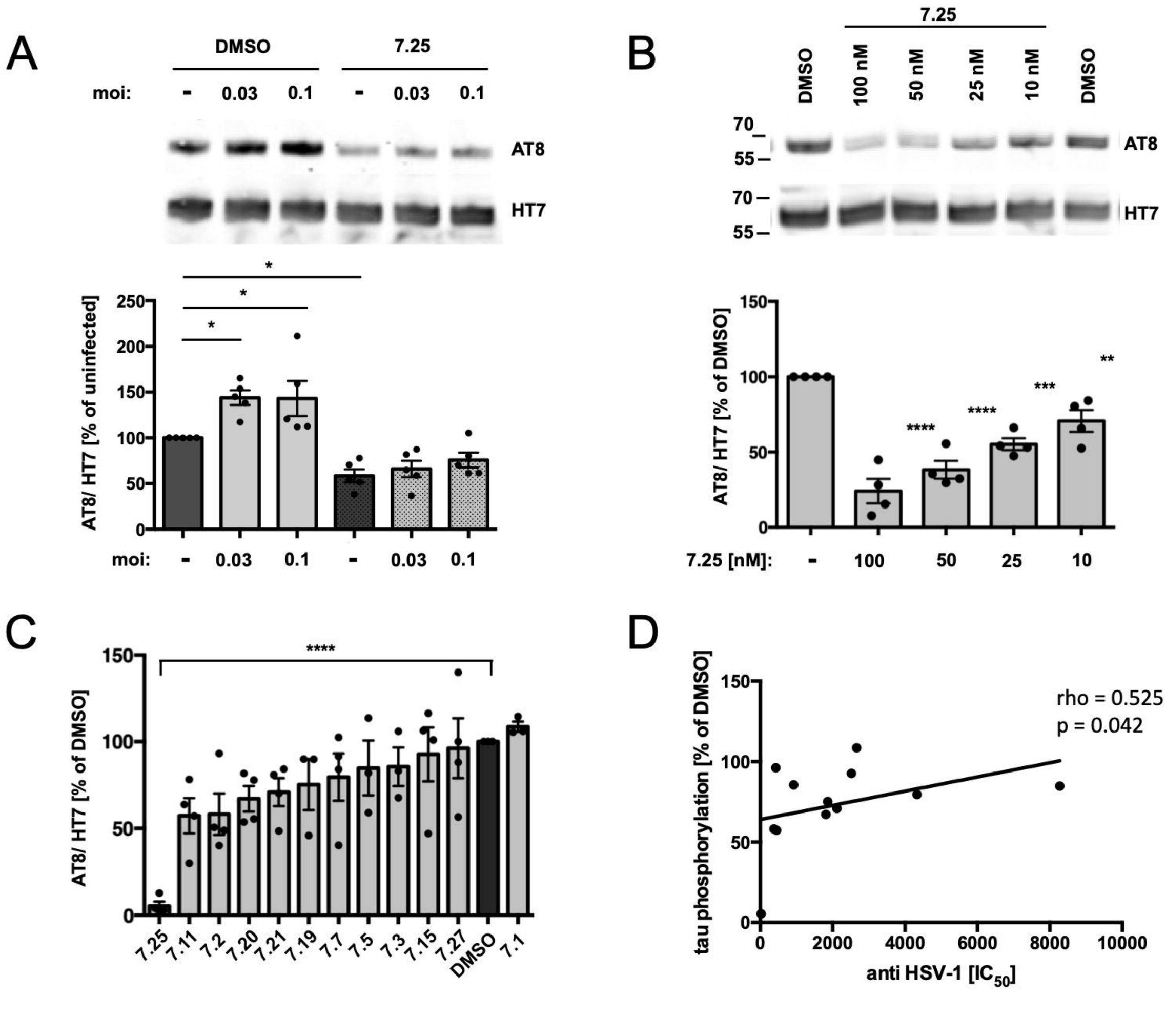

**Table 1**

A

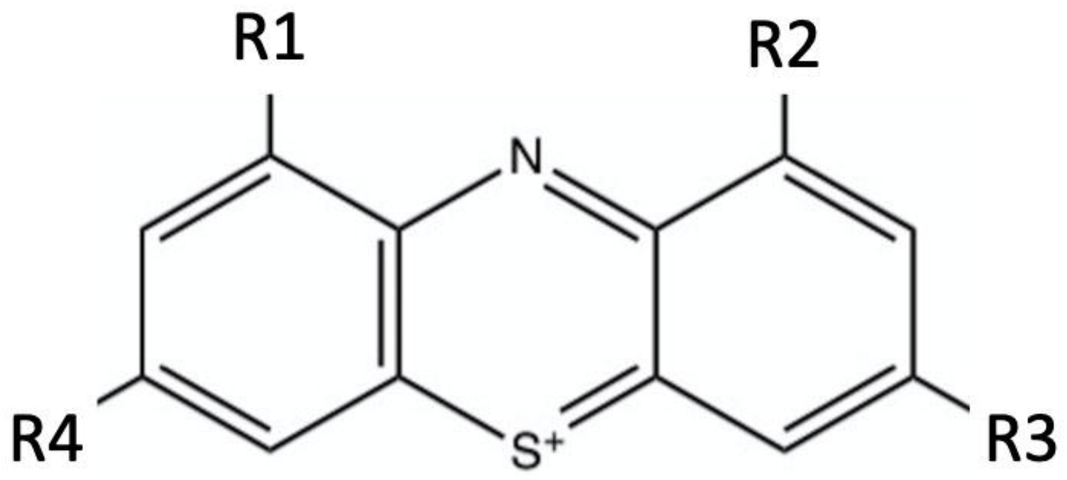


| # | R1 | R2 | R3 | R4 | $IC_{50}$ (μM) |
|---|---|---|---|---|---|
| **1.32** | | | 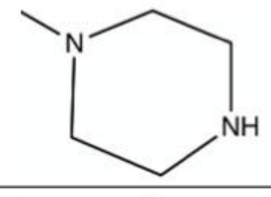 | 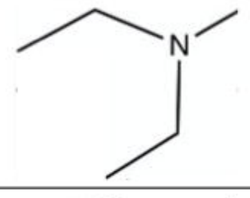 | 0.45 |
| **7.1** | | | 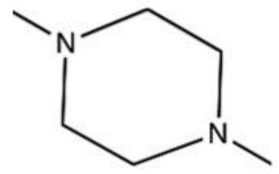 | 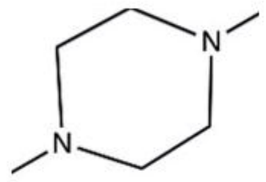 | 2.67 |
| **7.2** | | | 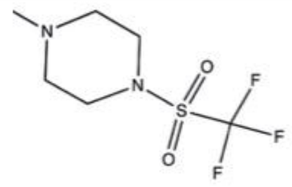 | 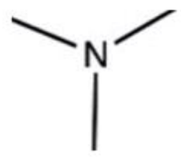 | 0.38 |
| **7.3** | | | 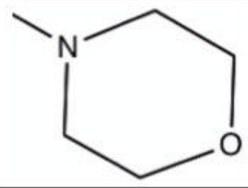 | 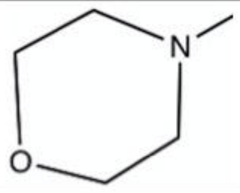 | 0.92 |
| **7.5** | | | 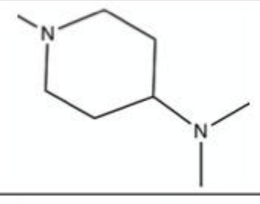 | 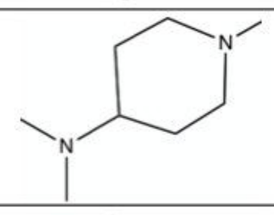 | 8.28 |
| **7.7** | | | 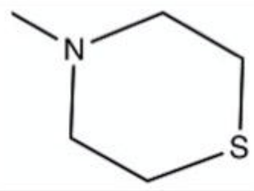 | 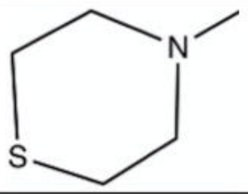 | 4.33 |
| **7.11** | | | 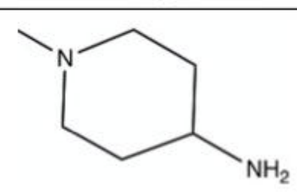 | 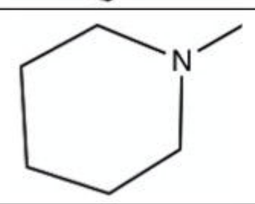 | 0.45 |
| **7.15** | | | 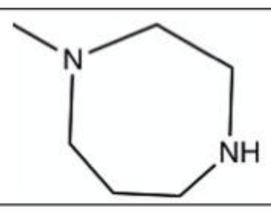 | 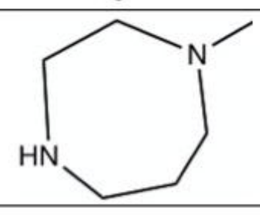 | 2.52 |
| **7.19** | | | 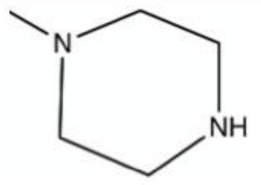 | 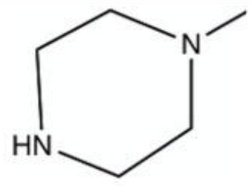 | 1.86 |
| **7.20** | | | 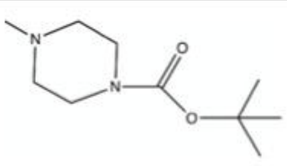 | 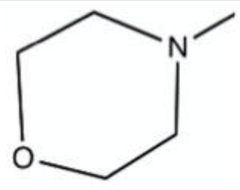 | 1.81 |
| **7.21** | | | 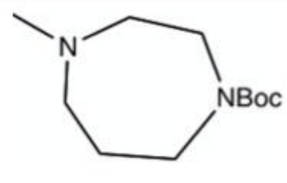 | 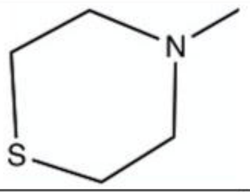 | 2.12 |
| **7.25** | | | 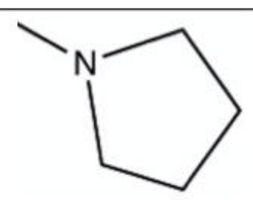 | 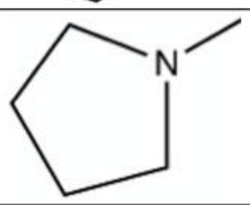 | 0.02 |
| **7.27** | | | 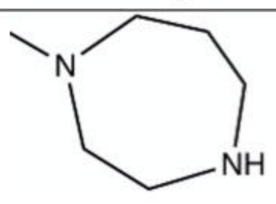 | 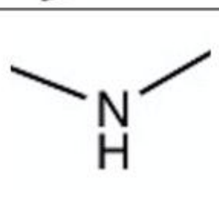 | 0.43 |

**Table 2**

| Protein name | MW (kDa) | Accession number | Peptides identified | Mascot ion score | % coverage |
|---|---|---|---|---|---|
| MIF | 12 | MIF_PIG | (M)PMFVVNTNVPR(A) | 51.5 | 17 |
| | | | (K)LLCGLLAER(L) | 60,9 | |
| cutA | 19 | F1RZR6_PIG | (K)GKIEEDSEVLMMIK(T) | 37,3 | 16 |
| | | | (K)IEEDSEVLMMIK(T) | 40,8 | |
| | | | (K)TQSSLVPALTDFVR(S) | 58,7 | |
| GSTP1 | 23 | GSTP1_PIG | (-)PPYTITYFPVR(G) | 56,5 | 27 |
| | | | (K)FQDGDLTLYQSNAILR(H) | 84,8 | |
| | | | (K)EAALVDMVNDGVEDLR(C) | 130,1 | |
| | | | (K)YATLIYTNYEAGK(E) | 41,4 | |
| PRDX2 | 22 | F1SDX9_PIG | (R)NLSLDYGVLKEDEGIAYR(G) | 55,5 | 15 |
| | | | (R)QITVNDLPVGR(S) | 57,2 | |
| PKM2 | 57 | F1SHL7_PIG | (R)NTGIICTIGPASR(S) | 56,5 | 7 |
| | | | (K)VYVDDGLISLLVK(Q) | 61,2 | |
| | | | (R)GDLGIEIPAEK(V) | 52,5 | |
| CALML3 | 12 | F1SQH2_PIG | (K)EAFSLFDK(D) | 59,6 | 42 |
| | | | (K)EAFSLFDKDGDGTITTK(E) | 73,4 | |
| | | | (K)DTDSEEEIREAFR(V) | 46,0 | |
| | | | (R)VFDKDGNGYISAAELR(H) | 77,3 | |
| | | | (R)VFDKDGNGYISAAELR(H) | 69,4 | |
| | | | (K)DGNGYISAAELR(H) | 63,7 | |
| HSPCB | 83 | F1RQU2_PIG | (R)TLTLVDTGIGMTK(A) | 70,3 | 5,4 |
| | | | (K)ADLINNLGTIAK(S) | 80,6 | |
| | | | (R)GVVDSEDLPLNISR(E) | 69,8 | |